Published in final edited form as:
Nanotechnology. 2013 January 18; 24(2): 025605. doi:10.1088/0957-4484/24/2/025605.

Fabrication and characterization of gold nano-wires templated on virus-like arrays of tobacco mosaic virus coat proteins

M Wnęk[1,5], **M Ł Górzny**[2,6], **M B Ward**[3], **C Wälti**[4], **A G Davies**[4], **R Brydson**[3], **S D Evans**[2], and **P G Stockley**[1]

[1]Astbury Centre for Structural Molecular Biology, University of Leeds, Leeds LS2 9JT, UK

[2]School of Physics and Astronomy, University of Leeds, Leeds LS2 9JT, UK

[3]Institute for Materials Research, SPEME, University of Leeds, Leeds LS2 9JT, UK

[4]School of Electronic and Electrical Engineering, University of Leeds, Leeds LS2 9JT, UK

Abstract

The rod-shaped plant virus tobacco mosaic virus (TMV) is widely used as a nano-fabrication template, and chimeric peptide expression on its major coat protein has extended its potential applications. Here we describe a simple bacterial expression system for production and rapid purification of recombinant chimeric TMV coat protein carrying C-terminal peptide tags. These proteins do not bind TMV RNA or form disks at pH 7. However, they retain the ability to self-assemble into virus-like arrays at acidic pH. C-terminal peptide tags in such arrays are exposed on the protein surface, allowing interaction with target species. We have utilized a C-terminal His-tag to create virus coat protein-templated nano-rods able to bind gold nanoparticles uniformly. These can be transformed into gold nano-wires by deposition of additional gold atoms from solution, followed by thermal annealing. The resistivity of a typical annealed wire created by this approach is significantly less than values reported for other nano-wires made using different bio-templates. This expression construct is therefore a useful additional tool for the creation of chimeric TMV-like nano-rods for bio-templating.

1. Introduction

One-dimensional (1D) nano-structures and nano-wires can serve as building blocks for ‘bottom-up’ nano-fabrication. They can function both as interconnecting wires and crucial device components, and as such can be used in the creation of various electronic, logic and memory circuits (see [1]). Self-assembling biological structures are proving to be highly promising templates for ordering inorganic materials into 1D nano-structures. They are hierarchically organized and possess highly specific and precise molecular recognition capabilities that often can be further programmed through genetic engineering (see [2]). A

[5]Present address: Institute of Infection and Global Health, University of Liverpool, Liverpool L69 7BE, UK.
[6]Present address: CIC nanoGUNE Consolider, Tolosa Hiribidea 76, E-20018 Donostia, San Sebastian, Spain.
p.g.stockley@leeds.ac.uk

Online supplementary data available from stacks.iop.org/Nano/24/025605/mmedia

Europe PMC Funders Author Manuscripts

major advantage of such bio-templated nano-structures is their ability to self-assemble spontaneously in a deterministic manner into functional arrangements without the need to manipulate each component individually. Various linear biomolecules such as DNA, amyloid fibers, microtubules and filamentous viruses have been successfully exploited as scaffolds for the construction of metal and semiconducting nano-wires [3–6].

Here we demonstrate the use of a genetically engineered tobacco mosaic virus (TMV) coat protein (CP) gene as a bio-template for the fabrication and characterization of gold nano-wires. TMV is a rod-shaped plant virus, comprising a single molecule of RNA enclosed within a capsid of ~2130 helically arranged protein subunits. The assembled virion particle is 300 nm long and 18 nm in diameter, with a 4 nm inner channel [7]. It is known to form many assembly intermediates in various pH ranges, including highly stable, elongated RNA-free helices in acidic conditions [8]. The capsid of a wild-type (WT) TMV contains a repeating array of surface-exposed charged amino acids [9]. A range of studies have reported the use of simple electrostatic interactions to bind various inorganic materials such as silica, platinum, nickel, cobalt, copper and gold, as well as the alloys CoPt and FePt to WT TMV [10–16]. Relatively little work, however, has been performed using genetically engineered TMV or TMV protein assemblies as a means of introducing new sequences for the directed and selective deposition of materials. Although this approach has been used to create gold, silver, platinum, palladium or nickel nano-wires, some of which have been characterized electrically [17–20], preparation of the biological template is complex and requires sophisticated biochemical knowledge.

In previous studies, we fabricated TMV-based platinum nano-wires via electroless deposition of platinum precursors onto the outer surface of the WT TMV virion. These wires were electrically characterized using a four-probe Omicron Nanoprobe system. Their Ohmic behavior was typical for a conducting wire that was capable of sustaining very high current densities [21]. However, such direct material deposition onto biological structures is mostly non-specific and depends strongly on the solution chemistry. As a result the nano-structures generated often exhibit poor crystalline, mechanical and electronic properties.

In order to address these constraints on the use of TMV as a well-ordered bio-template, we engineered the TMV CP to introduce a highly selective His-tag (HHHHHH, 6His) metal-binding peptide that would be readily accessible on the outer surface of assembled protein disks or rods. This was used for expression in *Escherichia coli*. Recombinant WT CP subunits form disks *in vivo* in this system but the His-tagged version did not. However, the His-tag allows rapid purification of this modified CP to homogeneity via standard nitrilotriacetic acid (NTA)-directed affinity chromatography. Treatment of TMV CP with low pH buffers triggers the formation of RNA-free helical protein rods with the geometry of the virion. Similar rods formed with both recombinant forms of the CP are produced here. The His-tagged rods, but not those formed from the recombinant WT protein, bind commercial gold nanoparticles (GNPs). Further deposition of metallic gold from solution was used to produce more uniformly coated structures. Thermal annealing of these ‘nano-wires’ produced more continuous gold coatings. These have been characterized by a variety of physical techniques, and their electrical properties assayed. This approach offers a

straightforward and highly reproducible method for chimera protein purification and formation of templates for nano-wire creation.

2. Experimental details

2.1. Preparation of genetically engineered TMV coat protein

WT and 6His versions of the TMV coat protein gene were created using reverse transcription and the polymerase chain reaction on a template of TMV RNA extracted from infectious virions. For PCR, forward and reverse gene-specific primers were used, which additionally introduced two restriction sites at the 5′ and 3′ ends of the CP gene, as well as a sequence for six histidine residues at the 3′ end of the 6His mutant (see supplemental information available at stacks.iop.org/Nano/24/025605/mmedia for details and primer sequences). The design results in the insertion of six C-terminal histidine residues at positions 159–164 of the TMV 6His CP. The WT and 6His genes were cloned into an expression vector and proteins expressed in *E. coli* BL21-CodonPlus cells. After overnight expression, cells were harvested and subjected to ultrasonic lysis. WT and 6His proteins were purified from soluble fractions of the lysates via size-exclusion chromatography (SEC) or Ni-NTA affinity chromatography, respectively. Purified WT and 6His samples were dialyzed against pH 8, pH 7 or pH 5 buffer for ‘A-protein’, ‘disk’ and re-assembly or RNA-free helix formation, respectively.

2.2. Electron microscopy

For protein and nano-wire investigation, samples were applied onto Formvar carbon-coated 300 mesh copper grids and stained with 2% (w/v) uranyl acetate, if required. Samples were imaged using a Philips CM10 transmission electron microscope (TEM) operated at 80 kV or a Philips CM200 FEG TEM operated at 197 kV.

2.3. GNP binding, metallic gold deposition and thermal annealing

WT and 6His virus-like particles (VLPs) were incubated with citrate-stabilized 2 or 5 nm GNPs for 1 h. UV photoreduction of gold ions was performed as described in [22]. For electroless gold deposition, VLPs were incubated with chloroauric acid and hydroxylamine for 10 min. For thermal annealing, a nano-wire sample applied onto a copper or silicon oxide TEM grid was heated in a vacuum until a desired temperature was reached, annealed at that temperature for 1 h, then slowly cooled to room temperature. This procedure was performed for different samples in 10 °C intervals in the temperature range of 200–300 °C.

2.4. Four-probe electrical characterization

Gold nano-wire samples were applied onto a silicon oxide grid and were either used directly for electrical conduction measurements (non-annealed NW) or subjected to the thermal annealing at 290 °C before electrical measurements (annealed NW). Electrical conductivity was measured in an ultra-high vacuum (UHV) chamber (2×10^{-10} mbar, room temperature) using the Omicron Nanoprobe.

Europe PMC Funders Author Manuscripts

3. Results and discussion

3.1. Cloning, expression and purification of His-tagged TMV rods

The TMV CP gene was cloned by RT-PCR of the virion RNA extracted from TMV virions, as described in the experimental details and supplementary information (available at stacks.iop.org/Nano/24/025605/mmedia). Two different primers were used to engineer differences at the 3′ end of the gene in the reverse transcription step. In the first (WT), the reverse primer is completely complementary to the WT gene and incorporates an *Nde*I cloning site. The second (6His) encodes an additional hexa-histidine peptide following the normal C-terminal residue, Thr158, and a *BamH*I restriction sites (figure 1(A)). The resultant PCR fragments were digested with *Nde*I and *BamH*I, cloned into a similarly prepared pET11c expression vector and used to transform BL21-CodonPlus-(DE3)-RIPL *E. coli.* This strain allows expression from transcripts containing codons rare in *E. coli*, many of which are found within the TMV CP gene. Isopropyl *β*-D-1-thiogalactopyranoside induction of both forms of CP resulted in high-level expression of products with the expected sizes (figure 1(B)). The His-tagged CP was easily purified to homogeneity by Ni-NTA chromatography. Mass spectrometry of this species confirms its identity (observed relative molecular mass (Mr) 18 316.7 Da; expected 18 315.3 Da) as having the additional six histidine residues but lacking the N-terminal acetylation that occurs in plants but not in *E.coli* [23–26]. The WT protein was purified by size-exclusion chromatography at pH 7 where it forms ‘disk’ intermediates. Mass spectrometry of this species confirms the lack of acetylation of the recombinant (observed Mr 17 493.47 Da versus 17 492.5 Da expected) compared to the material prepared from the virion (observed Mr 17 536.0 Da). The ~43 Da increase corresponds to the mass of a single acetyl group.

Wild-type TMV CP has a well-characterized pH-dependent ability to self-assemble into small oligomers (‘A-protein’), ‘disks’ composed of two stacked rings each of 17 subunits, and helical rods. The ‘disks’ are believed to be a principal intermediate during normal viral assembly triggered by a sequence-specific RNA–protein interaction [27]. Acetylation is believed to be essential for the RNA interaction [24, 25] and mixing the three forms of TMV CP with viral RNA under re-assembly conditions confirmed this, rod-shaped VLPs appearing in TEMs only for the CP extracted from virus (data not shown). In contrast to the recombinant WT CP, the 6His CP is unable to form ‘disks’ at pH 7, although at pH 8 both it and the recombinant wild-type appear as ‘A-protein’-like aggregates (supplemental figure 1(B) available at stacks.iop.org/Nano/24/025605/mmedia). Despite these differences from WT, both recombinant proteins formed long rods upon prolonged incubation in sodium acetate buffer at pH 5 (figures 1(C) and (D)). These appear to be RNA-free helices, which form as a result of protein polymerization into structures almost identical to the mature virus [28]. In such a structure the His-tags will be presented at the outer surface of the VLP (supplemental figure 1(A) available at stacks.iop.org/Nano/24/025605/mmedia), offering a rapid way to prepare rod-shaped templates for the production of nano-scale inorganic materials.

3.2. Derivatizing the His-tagged TMV rods with gold

As well as their ability to chelate nickel ions, poly-histidine peptides have been shown to recognize metallic gold in yeast-surface display experiments [29]. We therefore examined whether the 6His motif TMV VLPs would bind to GNPs. Treatment with citrate-stabilized GNPs (2 or 5 nm diameter) for 1 h at room temperature and pH 5, resulted in extensive decoration of the rods with GNPs (figures 2(A) and (B)). Unstained TEM images of these structures suggest that they contain GNPs bound at discrete sites rather than in clusters in direct contact, consistent with expectations of simple modeling (supplemental figure 1(D) available at stacks.iop.org/Nano/24/025605/mmedia). The GNP-coated rods appear slightly wider than the initial VLPs (25–30 nm versus 20 nm diameter) but had similar lengths (300–1200 nm) to the starting material, implying that they act as rigid templates for binding. Incubation of recombinant WT rods under similar conditions revealed no significant GNP binding (supplemental figure 1(C) available at stacks.iop.org/Nano/24/025605/mmedia), consistent with binding to the 6His motif. The numbers of GNPs bound varied with their sizes: ~100 for 2 nm GNPs and ~60 for 5 nm GNPs, on average/100 nm of each type of VLP. Even the 2 nm GNPs are not apparently close packed, although there is in principle enough room for them to be so assuming aggregates of stacked disks with 17 subunits per ring with a diameter of 20 nm and depth of 2.5 nm. The results are consistent with occlusion of the particles, possibly via electrostatic as well as steric constraints (figures 2(A) and (B), insets).

We then explored ways to create continuous gold wires from these GNP–VLP templates using the 2 nm GNP-coated rods since these have a more uniform distribution. A number of protocols (Nanoprobes GoldEnhance™ kit; [22, 30]) were examined to deposit metallic gold (Au^0) on these templates. Electroless deposition and UV photoreduction both resulted in metallic layers with the most homogeneous appearance (figure 2(C) and supplemental figure 1(E), available at stacks.iop.org/Nano/24/025605/mmedia, respectively). The apparently continuous nano-wires found after such treatments have average diameters of ~30–40 nm (for UV photoreduction) or ~50–60 nm (for electroless deposition). No deposition was seen for samples of GNP-free 6His or WT VLPs processed via either method (not shown). Although not obvious from supplemental figure 1(E) (available at stacks.iop.org/Nano/24/025605/mmedia) exposure to UV light resulted in degradation of the protein scaffold causing the wires to break. In addition, high levels of background material were observed on the micrographs, which could potentially interfere with electrical measurements. As a consequence, the more uniform wires created via electroless deposition were chosen for further analysis.

3.3. Thermal annealing

These wires were then examined via high-resolution transmission electron microscopy (HRTEM), energy dispersive x-ray spectroscopy (EDX) and selected area electron diffraction (SAED). These data revealed that the wires were highly polycrystalline, consisting of face-centered cubic crystals of approximate size 5 nm [31]. Since such polycrystalline material is likely to possess a higher resistivity than larger grained material, we then examined the effect of thermal annealing on the gold layer. Grain growth was promoted via thermal annealing, which reduces polycrystallinity and hence improves

Europe PMC Funders Author Manuscripts

electrical properties [32]. Reduction and growth of new grain boundaries are events that strongly depend on parameters such as temperature and the duration of the heating, annealing and cooling steps. In our experiments, 60 min annealing *in vacuo*, followed by slow cooling was performed to facilitate local crystal rearrangements, the formation of large grains and minimization of oxidation. The best temperature for the annealing step was established by TEM inspection of wires heated at a range of temperatures (200–300 °C)

As shown in figure 3(B), heating and annealing at all temperatures below 270 °C led to disruption of the wires into a series of discrete gold crystallites. As the annealing temperature increased, however, the number and sizes of the interparticle gaps decreased whilst the length of the uninterrupted metallic layer increased. The average diameter of the annealed nano-wires also decreased (figure 3(B)). Annealing at 290 °C resulted in the longest and thinnest apparently continuous wires, with mean length of 650±60 nm and average diameter of ~40 nm.

Their thinner appearance compared to non-annealed nano-wires is most probably due to loss of the underlying protein scaffold, which has most likely been converted to amorphous carbon during the annealing process. HRTEM confirmed this idea, the 6His VLP being easily distinguishable in the non-annealed nano-wire beneath the metallic layer (figure 3(A)), and no longer visible after annealing at 290 °C (figure 3(C)). In addition, differences in the overall appearance and crystal nature of the nano-wires were observed. As expected the number of small crystals in the non-annealed nano-wire (figure 3(A) inset) was significantly reduced after the thermal processing (figure 3(C) inset). EDX confirmed that the annealed metal layer was composed of gold, although the spectrum had an additional oxygen peak suggesting possible oxidation (supplemental figure 1(I) available at stacks.iop.org/Nano/24/025605/mmedia). This was confirmed via SAED, which showed reflections in the diffraction pattern characteristic of gold oxide Au_2O_3 [33].

3.4. Electrical characterization of the nano-wires

We next characterized the annealed and non-annealed nano-wires electrically using an Omicron Nanoprobe. This instrument comprises a set of four custom designed, independently positioned scanning tunneling microscope (STM) tips, with an average diameter at the tip apex of less than <25 nm [34]. In addition, the Nanoprobe system includes a Gemini high-resolution scanning electron microscope (SEM), which provides a resolution of better than 10 nm. This was employed to locate the nano-wires and navigate the STM tips to a desired region. The components of the Nanoprobe system are located within an UHV chamber, which shields them from the electrical, thermal and vibrational influences [35].

Using the Nanoprobe system, we performed two-probe conductivity measurements on both types of TMV gold nano-wires. A representative example of each type of TMV nano-wire was analyzed and the results are shown in figure 4. The non-annealed nano-wire was 1320 nm long and 60 nm in diameter (figure 4(A)). The annealed nano-wire was 930 nm long and 40 nm in diameter (figure 4(C)). For the conductivity measurements, two STM probes were brought into contact with the surface of the nano-wire. Current–voltage (*I–V*) characteristics of the wires were measured by sweeping the current while measuring the voltage drop

between tips T1 and T2. A number of *I–V* curves for different tip separations were measured by varying the positions of one of the tips (figures 4(A) and (C)). Five and eight sweeps were taken for the non-annealed and annealed wire, respectively. In all cases, the *I–V* characteristics were linear, consistent with the behavior expected for an Ohmic conductor (figures 4(B) and (D), left). The contribution to the charge transport from the silicon support was negligible (figures 4(B) and (D), left insets).

From the *I–V* measurements, the resistance *R* for each individual probe distance *L* was calculated and the results are shown in figures 4(B) and (D) (right). The measured resistances include the resistance of the wire plus the two contact resistances between the tips and the wire. For the non-annealed nano-wire, *R* varies exponentially with the separation between the tips and extrapolation to zero length suggests a total contact resistance of around 70 Ω (figure 4(B), right). The exponential dependence may suggest that the wire is non-continuous and is in fact made up of an array of small metallic stretches of wire joined by tunnel contacts. Despite this, the wire seems to be reasonably homogeneous as the number of tunnel contacts seems to increase pro-rata with the length of the wire.

This is in contrast to the annealed nano-wire, where no correlation between tip separation and resistance was observed (figure 4(D), right). This suggests that in this case the resistance is entirely dominated by the contact resistances. The contact resistances seem to be much larger than for the non-annealed nano-wires, probably as a result of surface oxidation during the high-temperature treatment. The upper limit of the resistivity of the annealed nano-wire can be estimated by assuming that the contributions from the contacts are negligible, and hence that the measurements are dominated by the contributions from the wire itself. The diameter of the wire is on average around 40 nm, and using the measured resistance at L = 715 nm, an upper limit of the resistivity of the nano-wire of $\rho = 4 \times 10^{-7}$ Ω m is found. This is less than 20 times higher than the resistivity of bulk gold ($\rho_{\text{bulk gold}} = 2.05 \times 10^{-8}$ Ω m measured at room temperature [36]). This value is significantly lower than previously reported resistivities of gold nano-wires created using different bio-templates, which are typically two orders of magnitude higher than bulk gold [5, 30, 37, 38]. We note that the real resistivity is likely to be significantly lower than the upper limit determined above, given that the contact resistances are in fact not negligible. Furthermore, we have investigated the maximum current density the nano-wire can sustain by increasing the applied bias voltage across the wire until it disintegrated. A current of around 1.6 mA could be sustained for several minutes, which corresponds to a current density of around 1.3×10^{12} A m^{-2}. This compares well with previous studies of nano-wires where similar breakdown currents were reported [39].

4. Conclusions

It can be argued that self-assembling 1D nano-structures and nano-wires will play an important role as future device elements to complement the constantly miniaturizing electronics industry. Here we have demonstrated that a His-tagged TMV helical VLP shows great potential as a scaffold for the controlled fabrication of gold nano-wires. The introduction of simple genetic modifications enabled the specific attachment of GNPs onto the VLP template, while at the same time providing a quick, one-step purification of the

Europe PMC Funders Author Manuscripts

protein subunits that needs little specialist knowledge. The fabricated TMV helix-based gold nano-wires were shown to be conductive, and, once thermally annealed, yielded resistivities much smaller than previously reported for other bio-templated nano-wires. Furthermore, they were able to sustain high current densities, which makes them highly suitable as components of nanometer-scale electronic devices. This simple method of incorporation of specific binding peptides into the structure of VLPs can be easily modified to encompass a wide range of other inorganic materials. We have shown that the exploitation of self-assembling TMV structures and introduction of programmable genetic control over material composition provides a means of generating a simple, yet highly ordered, template for the general synthesis of device components.

Supplementary Material

Refer to Web version on PubMed Central for supplementary material.

Acknowledgments

We wish to thank Dr Marc van Regenmortel (University of Strasbourg, France) for providing us with the wild-type TMV virus and Dr George Lomonossoff (John Innes Centre, Norwich) for helpful discussions. This work was supported in part by the UK EPSRC EP/H007334/1 and EP/C006755/1 (Basic Technology Programme), the University of Leeds Institute of Bionanosciences and the Wellcome Trust via their support of the facilities used [062164][090932/Z/09/Z]. We also acknowledge support from the Royal Society and the Wolfson Foundation.

References

[1]. Mbindyo JKN, Mallouk TE, Mattzela JB, Kratochvilova I, Razavi B, Jackson TN, Mayer TS. Template synthesis of metal nanowires containing monolayer molecular junctions. J. Am. Chem. Soc. 2002; 124:4020–6. [PubMed: 11942840]

[2]. Zhang S. Fabrication of novel biomaterials through molecular self-assembly. Nature Biotechnol. 2003; 21:1171–8. [PubMed: 14520402]

[3]. Gu Q, Cheng C, Gonela R, Suryanarayanan S, Anabathula S, Dai K, Haynie DT. DNA nanowire fabrication. Nanotechnology. 2006; 17:R14–25.

[4]. Malisauskas M, Meskys R, Morozova-Roche LA. Ultra thin silver nanowires produced by amyloid biotemplating Biotechnol. Prog. 2008; 24:1166–70.

[5]. Zhou JC, et al. Microtubule-based gold nanowires and nanowire arrays. Small. 2008; 4:1507–15. [PubMed: 18752207]

[6]. Lee Y-J, Yi H, Kim W-J, Kang K, Yun DS, Strano MS, Ceder G, Belcher AM. Fabricating genetically engineered high-power lithium-ion batteries using multiple virus genes. Science. 2009; 324:1051–5. [PubMed: 19342549]

[7]. Van Regenmortel, MHV.; Fraenkel-Conrat, H. The Plant Viruses: The Rod-shaped Plant Viruses. Vol. 2. Kluwer Academic; Dordrecht: 1986.

[8]. Butler PJG. Self-assembly of tobacco mosaic virus: the role of an intermediate aggregate in generating both specificity and speed. Phil. Trans. R. Soc. B. 1999; 354:537–50. [PubMed: 10212933]

[9]. Shenton W, Douglas T, Young M, Stubbs G, Mann S. Inorganic–organic nanotube composites from template mineralization of tobacco mosaic virus. Adv. Mater. 1999; 11:253–6.

[10]. Knez M, Sumser M, Bittner AM, Wege C, Jeske H, Martin TP, Kern K. Spatially selective nucleation of metal clusters on the tobacco mosaic virus. Adv. Funct. Mater. 2004; 14:116–24.

[11]. Balci S, Bittner AM, Hahn K, Scheu C, Knez M, Kadri A, Wege C, Jeske H, Kern K. Copper nanowires within the central channel of tobacco mosaic virus particles Electrochim. Acta. 2006; 51:6251–7.

[12]. Tseng RJ, Tsai C, Ma L, Ouyang J, Ozkan CS, Yang Y. Digital memory device based on tobacco mosaic virus conjugated with nanoparticles. Nature Nanotechnol. 2006; 1:72–7. [PubMed: 18654145]

[13]. Tsukamoto R, Muraoka M, Seki M, Tabat H, Yamashita I. Synthesis of CoPt and $FePt_3$ nanowires using the central channel of tobacco mosaic virus as biotemplate. Chem. Mater. 2007; 19:2389–91.

[14]. Bromley KM, Patil AJ, Perriman AW, Stubbs G, Mann S. Preparation of high quality nanowires by tobacco mosaic virus templating of gold nanoparticles. J. Mater. Chem. 2008; 18:4796–801.

[15]. Royston ES, Brown AD, Harris MT, Culver JN. Preparation of silica stabilized tobacco mosaic virus templates for the production of metal and layered nanoparticles. J. Colloid Interface Sci. 2009; 332:402–7. [PubMed: 19159894]

[16]. Balci S, Hahn K, Kopold P, Kadri A, Wege C, Kern K, Bittner AB. Electroless synthesis of 3 nm wide alloy nanowires inside tobacco mosaic virus. Nanotechnology. 2012; 23:045603. [PubMed: 22214553]

[17]. Lee S-Y, Royston E, Culver JN, Harris MT. Improved metal cluster deposition on a genetically engineered tobacco mosaic virus template. Nanotechnology. 2005; 16:435–41.

[18]. Lee S-Y, Choi J, Royston E, Janes DB, Culver JN, Harris MT. Deposition of platinum clusters on surface-modified tobacco mosaic virus. J. Nanosci. Nanotechnol. 2006; 6:974–81. [PubMed: 16736753]

[19]. Royston E, Ghosh A, Kofinas P, Harris MT, Culver JN. Self-assembly of virus-structured nanomaterials and their application as battery electrodes. Langmuir. 2008; 24:906–12. [PubMed: 18154364]

[20]. Kadri A, Maiß E, Amsharov N, Bittner AM, Balci S, Kern K, Jeske H, Wege C. Engineered tobacco mosaic virus mutants with distinct physical characteristics in planta and enhanced metallization properties. Virus Res. 2011; 157:35–46. [PubMed: 21310199]

[21]. Górzny ML, Walton AS, Wnęk M, Stockley PG, Evans SD. Four-probe electrical characterization of Pt-coated TMV-based nanostructures. Nanotechnology. 2008; 19:165704. [PubMed: 21825656]

[22]. Zhou J, Gao Y, Lau J, Hamasaki T, Hu E, Dunn B. Nanoscale assembly of gold nanowires templated by microtubules. J. Phys.: Conf. Ser. 2007; 61:1352–6.

[23]. Filner B, Marcus A. TMV coat protein synthesis *in vivo*: analysis of the *N*-terminal acetylation. Virology. 1974; 61:537–46. [PubMed: 4418398]

[24]. Hwang D-J, Roberts IM, Wilson MA. Expression of tobacco mosaic virus coat protein and assembly of pseudovirus particles in Escherichia coli. Proc. Natl Acad. Sci. USA. 1994a; 91:9067–71. [PubMed: 8090770]

[25]. Hwang D-J, Roberts IM, Wilson MA. Assembly of tobacco mosaic virus and TMV-like pseudovirus particles *Escherichia coli*. Arch. Virol. Suppl. 1994b; 9:543–58. [PubMed: 7518274]

[26]. Polevoda B, Sherman F. N-terminal acetyl transferases and sequence requirements for N-terminal acetylation of eukaryotic proteins. J. Mol. Biol. 2003; 325:595–622. [PubMed: 12507466]

[27]. Butler PJG, Klug A. Assembly of the particle of tobacco mosaic virus from RNA and disks of protein. Nature New Biol. 1971; 229:47–50. [PubMed: 5276072]

[28]. Madelkow E, Stubbs G, Warren S. Structures of the helical aggregates of tobacco mosaic virus protein. J. Mol. Biol. 1981; 152:375–86. [PubMed: 7328658]

[29]. Peele BR, Krauland EM, Wittrup KD, Belcher AM. Design criteria for engineering inorganic material-specific peptides. Langmuir. 2005; 21:6929–33. [PubMed: 16008405]

[30]. Huang Y, Chiang C-Y, Lee SK, Gao Y, Hu EL, Yoreo JD, Belcher AM. Programmable assembly of nanoarchitectures using genetically engineered viruses. Nano Lett. 2005; 5:1429–34. [PubMed: 16178252]

[31]. Joint Committee on Powder Diffraction Standards. reference code 00-004-0784.

[32]. Porath D, Goldstein Y, Grayevsky A, Millo O. Scanning tunnelling microscopy studies of annealing of gold films. Surf. Sci. 1994; 321:81–8.

[33]. Joint Committee on Powder Diffraction Standards. reference code 00-043-1039.

[34]. McKendry JE, Allen CS, Critchley K, Górzny MŁ, Walton AS, Evans SD. Magnetic field enhanced nano-tip fabrication for four-probe STM studies. Nanotechnology. 2008; 19:085201. [PubMed: 21730719]

[35]. Lin X, He X, Lu J, Gao L, Huan Q, Deng Z, Cheng Z, Shi D, Gao H. Manipulation and four-probe analysis of nanowires in UHV by application of four tunneling microscope tips: a new method for the investigation of electrical transport through nanowires. Surf. Interface Anal. 2006; 38:1096–102.

[36]. Lide, DR. Handbook of Chemistry and Physics. CRC Press; Boca Raton, FL: 1997.

[37]. Valizadeh S, Abid M, Hernandez-Ramirez F, Rodriguez AR, Hjort K, Schweitz JA. Template synthesis and forming electrical contacts to single Au nanowires by focused ion beam techniques. Nanotechnology. 2006; 17:1134–9. [PubMed: 21727393]

[38]. Joshi RK, West L, Kumar A, Joshi N, Alwarappan S, Kumar A. Production of semiconducting gold–DNA nanowires by application of DC bias. Nanotechnology. 2010; 21:185604. [PubMed: 20388979]

[39]. Karim S, Maaz K, Ensinger W. Diameter dependent failure current density of gold nanowires. J. Phys. D: Appl. Phys. 2009; 42:185403.

Europe PMC Funders Author Manuscripts

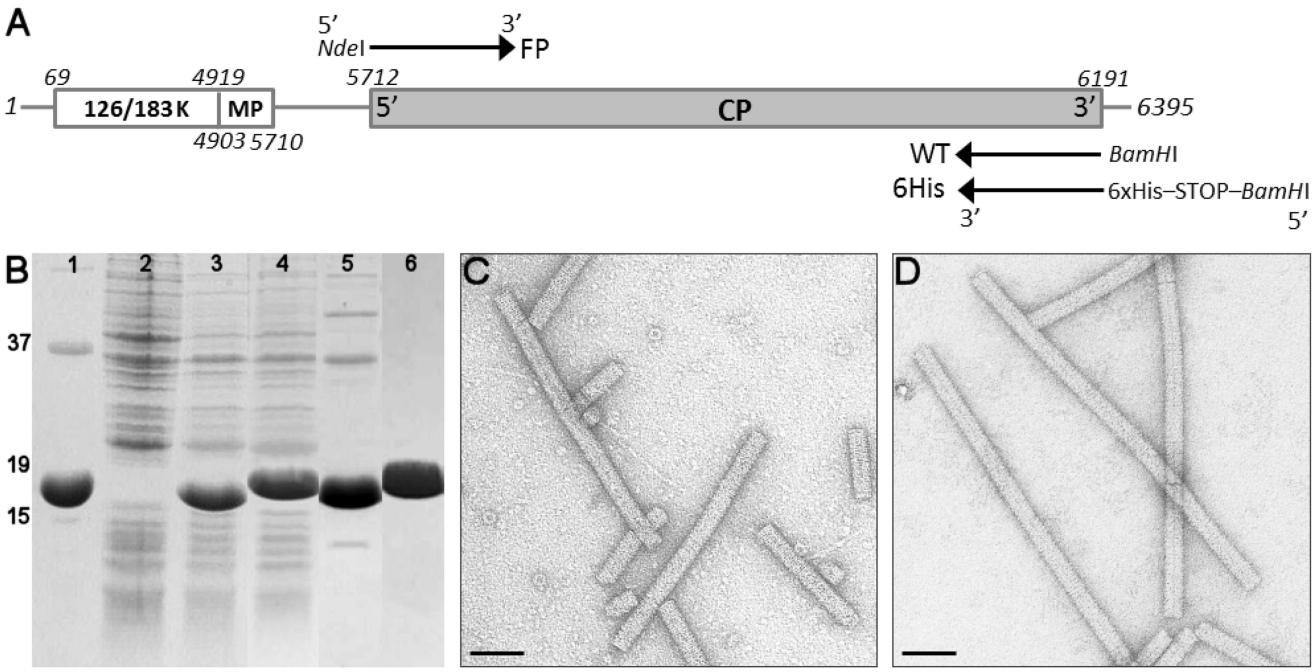

Figure 1.

Cloning, expression and characterization of TMV coat proteins. (A) TMV genome organization and primer attachment sites. Lines represent non-coding regions, coding regions are boxed and TMV coat protein is represented by a gray box, in which 5′ and 3′ termini are marked. Forward primer FP with a mismatched sequence for the *Nde*I restriction site is shown above the CP coding region, two variants of reverse primers, WT with mismatched sequence for the *BamH*I restriction site and 6His with mismatched sequence for six histidine residues, translation termination and *BamH*I site, are both shown below the CP coding region. (B) Coomassie-stained sodium dodecyl sulfate polyacrylamide gel electrophoresis of the *E. coli* expressed WT and 6His proteins. Lanes: 1, virion coat protein; 2, non-induced control; 3, overnight expression of WT protein; 4, overnight expression of 6His protein; 5, SEC purification of WT protein; 6, Ni-NTA purification of 6His protein. Size markers of 15, 19 and 37 kDa are indicated on the left. (C) TEM of WT coat protein polymerization into RNA-free rods at pH 5. (D) TEM of 6His-coat protein polymerization into RNA-free rods at pH 5. All stained. Scale bars = 50 nm.

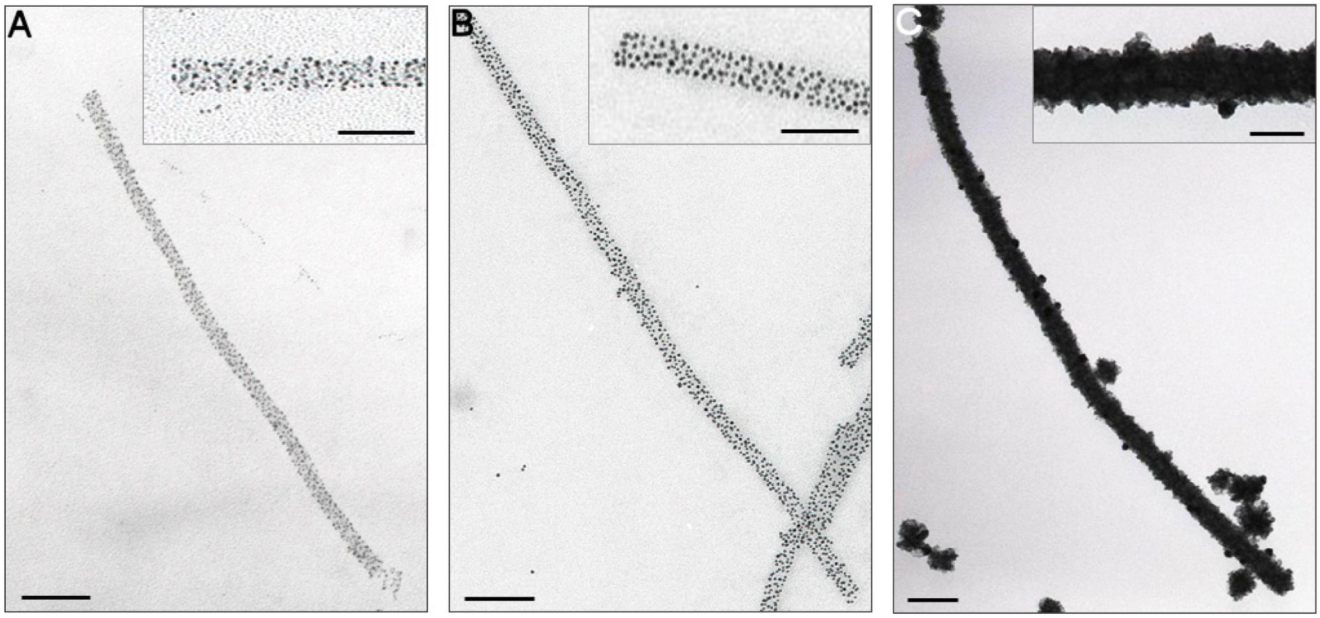

Figure 2.

Decoration of TMV VLPs with gold. (A) 6His VLP treated with 2 nm GNPs. Insets here and throughout show a 2 × magnification of the main images. (B) 6His VLP treated with 5 nm GNPs. (C) 2 nm GNP-treated 6His VLP subjected to electroless gold deposition. All images are unstained. Main scale bars = 100 nm, inset = 50 nm.

Europe PMC Funders Author Manuscripts

Europe PMC Funders Author Manuscripts

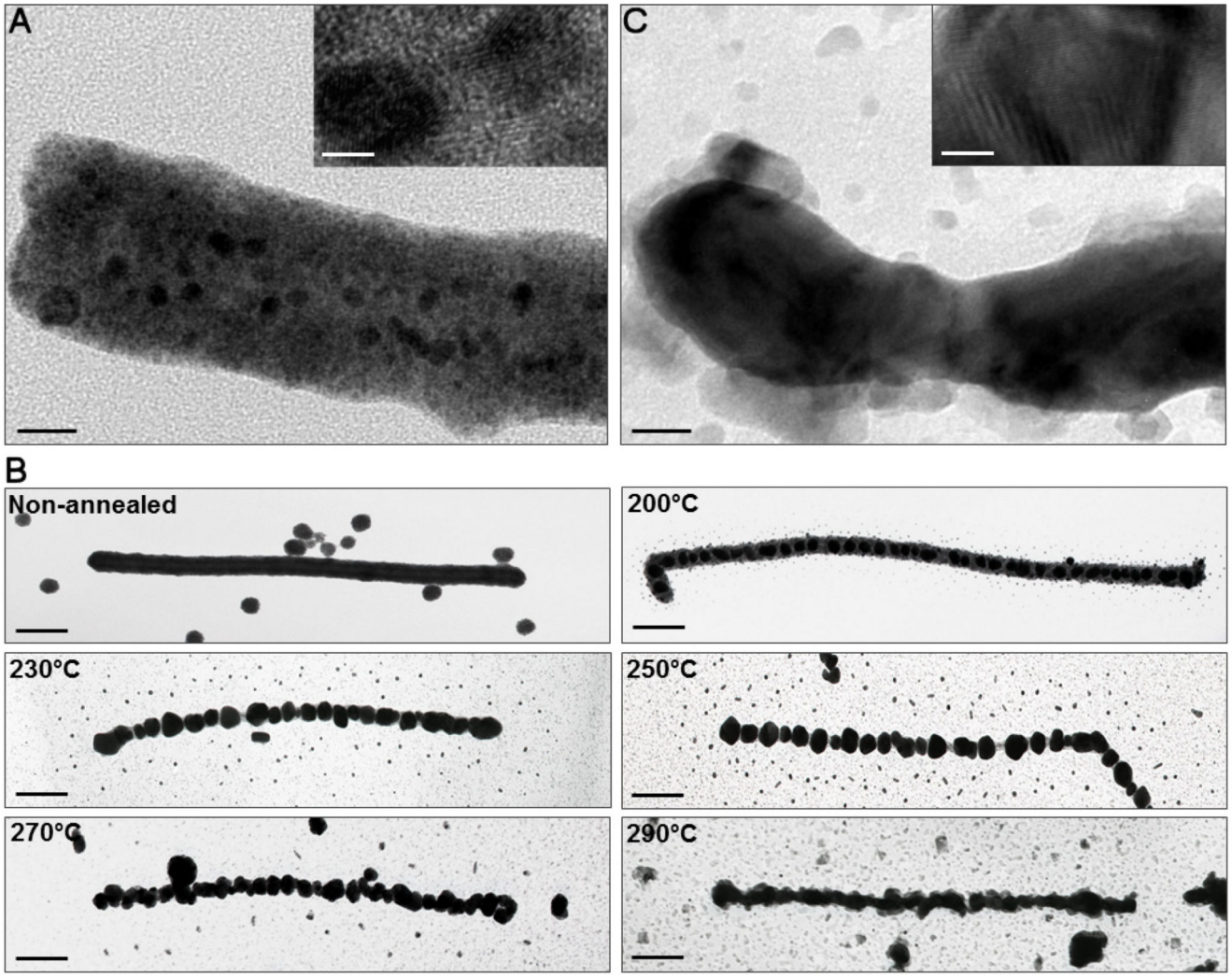

Figure 3.

Physical characterization of bio-templated nano-wires. (A) HRTEM of the 2 nm GNP-treated 6His VLP subjected to electroless gold deposition (non-annealed nano-wire) (scale bar = 20 nm). Inset: magnification of the non-annealed nano-wire showing multiple gold crystals. (B) Thermal annealing of the gold nano-wires. Nano-wires were subjected to electroless gold deposition and annealed for 1 h at temperatures between 200 and 300 °C (scale bars = 100 nm). (C) HRTEM of a gold nano-wire annealed at 290 °C (scale bar = 20 nm). Inset: magnification of the annealed nano-wire showing a single, large gold crystal.

Europe PMC Funders Author Manuscripts

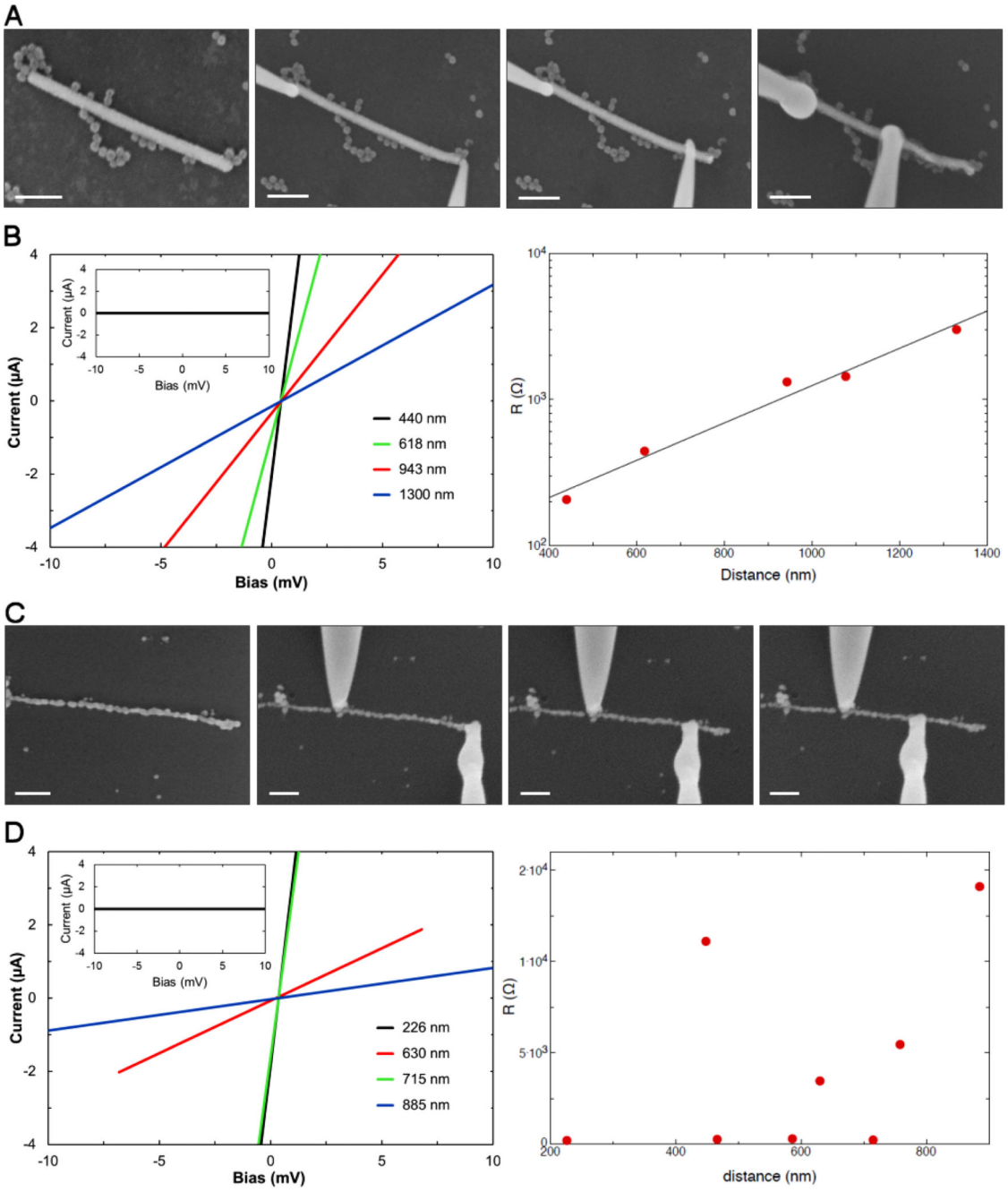

Figure 4.

Electrical characterization of the bio-templated nano-wires. (A) SEM images of two-probe electrical transport measurement setup of the non-annealed gold nano-wire performed with a tip separation between 1300 and 440 nm. All unstained. Scale bars = 200 nm. (B) Left: *I–V* characteristics of the non-annealed gold nano-wire for different tip separations. Inset: *I–V* characteristics of the silicon substrate; right, resistance versus tip separation (R–L) of the non-annealed nano-wire. (C) SEM images of two-probe electrical transport measurement setup of the annealed gold nano-wire performed with the tip separation between 885 and 226

nm. All unstained. Scale bars = 200 nm. (D) Left: *I*–*V* characteristics of the annealed gold nano-wire for a selection of different tip separations. Inset: *I*–*V* characteristics of the silicon substrate; right, resistance versus tip separation (R–L) of annealed nano-wire.

Europe PMC Funders Author Manuscripts